Astron. Astrophys. 337, 477–486 (1998)

ASTRONOMY AND ASTROPHYSICS

Optimizing the opacity sampling method

Christiane Helling[1,2] **and Uffe Gråe Jørgensen**[1]

[1] Niels Bohr Institute, University Observatory, Juliane Maries Vej 30, DK-2100 Copenhagen, Denmark
[2] Institute for Astronomy and Astrophysics, Technical University Berlin, Hardenbergstrasse 36, D-10623 Berlin, Germany

Received 12 September 1997 / Accepted 2 June 1998

Abstract. Modern computers allow solutions of the radiative transfer problem at a large number of frequencies during the iterative process of computing a detailed line-blanketed hydrostatic model atmosphere. However, the computing time increases approximately linearly with the number of frequency points. For computationally more complex and time-consuming problems, such as dust driven winds or pulsating AGB stars, it is therefore often not feasible to solve the radiative transfer problem for more than a single (i.e. mean or constant opacity) or a very modest number of frequencies. This paper analyzes how to optimize the selection of frequency points in particular when solving the radiative transfer problem at a very small number of points. We compute opacity sampled hydrostatic model atmospheres based on a large number of opacity sampling frequency points (of the order of 10.000), and successively reduce the number of frequencies in order to quantify the statistical error in the model structure introduced by a too coarse sampling. The results are compared to hydrostatic model atmospheres obtained by using other opacity approximations (Rosseland mean, straight means, constant opacity). We conclude that a considerable improvement in the accuracy of the model structure over such approximations can be achieved with a very modest number (20 - 50) of sampling frequencies, and give recommendations on how to choose the frequencies optimally.

Key words: radiative transfer – methods: statistical – stars: atmosphere – stars: giants

1. Introduction

Models of stellar atmospheres provide the main tool for the physical understanding and the interpretation of observed light from stars. Non-grey radiative transfer models (Gustafsson et al. 1975, Kurucz 1979, Brown et al. 1989, Jørgensen et al. 1992, Plez et al. 1992) allow for a reliable determination of the atmospheric structure and the atomic and molecular abundances in the photosphere. The very complex hydrodynamic models of dusty envelopes of pulsating stars (Fleischer et al. 1992, Höfner et al. 1997) can be used for the prediction of mass loss rates and the interpretation of light curves (Winters et al. 1994, Winters et al. 1997). However, such time-dependent models use a simplified (grey) treatment of the radiative transfer problem because of limited CPU time and lack of opacity data. A special problem of using the grey approximation arises when determining the effective temperature in e.g. stellar evolutionary models (VandenBerg et al. 1983, Salaris 1993).

The quality of the treatment of the radiative transfer problem has a strong influence on the resulting thermodynamical structure of a stellar atmosphere. Approximate techniques for the solution of the radiative transfer problem, e.g. using mean opacities, typically lead to errors of the order of a few 100 K (cf. Sect. 5). Such temperature errors can easily change the molecular concentrations by orders of magnitudes. Concerning the dust forming objects, such a temperature error may lead to a different efficiency of dust formation and, thus, to a different structure and dynamical behaviour of the shell, including important observational quantities like the mass loss rate and terminal wind velocities.

The opacity sampling (OS) technique (e.g. Carbon 1984, Ekberg et al. 1986) accomplishes high accuracy by using an adequate distribution of a sufficient number of points in the wavenumber space. For cool stars, where millions of molecular lines dominate the radiative transfer (particularly in the upper photospheric layers), the OS statistical approach will lead to the most convenient and accurate atmospherical computation (Sneden et al. 1976, Jørgensen et al. 1992, Plez et al. 1992). It has not been clear where the optimum distribution of sampling points lies, especially when going to a smaller and smaller number of points.

In this paper, we explore the reliability of the radiative transfer solution in hydrostatic model atmospheres of cool giant stars applying the OS technique with a decreasing number of sampling points down to a very modest number of ≈ 20 points. We study the resulting change in the atmospheric structure, and determine the minimum number of sampling points which still satisfies the statistical approach of the OS method. To accomplish this, we compare the model computations to an elaborate reference model calculated by means of a large number ($\approx 22\,000$ in the oxygen-rich case and $\approx 5\,300$ in the carbon-rich case) of wavenumber points. We calculate the error introduced by fewer and fewer sampling points, and demonstrate the large deviations

Send offprint requests to: Ch.Helling, (helling@stella.nbi.dk)

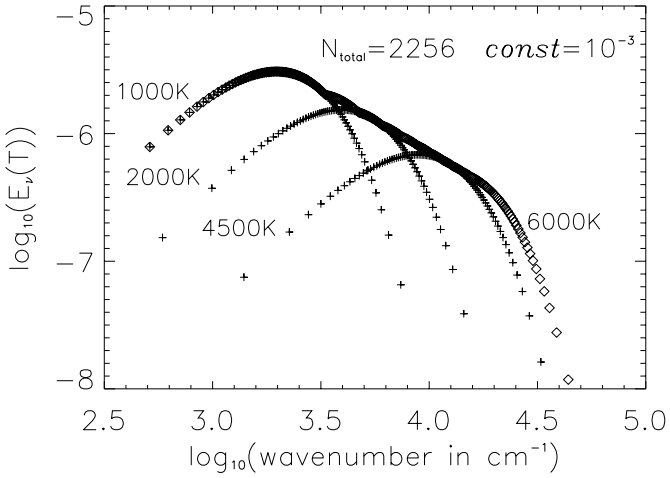

Fig. 1. Initial Planckian distributions (crosses) for selected $T_{\rm OS}$ and their "covering" curve (open diamonds, 2 256 points with $const = 10^{-3}$).

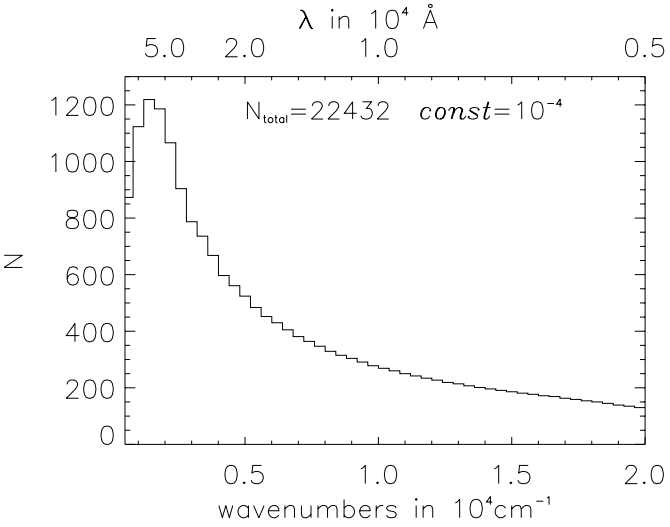

Fig. 2. The histogram for the final sampling point distribution with 22 432 sampling points ($const = 10^{-4}$).

which occur when using a mean opacity or even a constant opacity value.

2. Distribution of the opacity sampling points

The frequency distribution of the mean intensity at every depth in the atmosphere can roughly be approximated by the Planckian of a suitable temperature. Peytremann (1974) for the first time used a Planckian sampling point distribution. Gustafsson et al. (1975) (see also Ekberg et al. 1986) showed that in radiative and thermal equilibrium the temperature error can be minimized if the distribution function of sampling points is proportional to a Planck distribution.

However, it is not obvious which temperature $T_{\rm OS}$ to choose for the Planck function, since the temperature is a function of depth in the atmosphere. A choice of a relatively high temperature will under-sample the important long-wavelength regions in the upper cooler layers, and vice versa. Therefore, one optimally should use different Planck distributions at different depth layers.

Up to now, sampling points have been distributed according to one Planck function with $T_{\rm OS} = T_{\rm eff}$. We apply a new concept of Planckian distributed sampling points according to a (particular) temperature range from 1000 K to 6000 K.

The radiative energy density of a black body at temperature T [K] as function of wavenumber $\tilde{\nu}$ [1/cm] is

$$u(T,\tilde{\nu})\ d\tilde{\nu} = 8\pi hc\ \frac{\tilde{\nu}^3}{e^{h\tilde{\nu}c/kT}-1}\ d\tilde{\nu}, \tag{1}$$

and the normalized energy density per wavenumber interval at temperature T

$$E_{\tilde{\nu}}(T)\ d\tilde{\nu} = \frac{u(T,\tilde{\nu})}{4\sigma_{\rm SB}T^4/c}\ d\tilde{\nu}, \tag{2}$$

with $\sigma_{\rm SB}$ being the Stefan-Boltzmann constant, k the Boltzmann constant, and c the speed of light. To equalize the energies in all wavenumber intervals $\Delta\tilde{\nu}$, we write

$$\Delta E(T) = \int_{\tilde{\nu}}^{\tilde{\nu}+\Delta\tilde{\nu}} E_{\tilde{\nu}}(T)\ d\tilde{\nu} \stackrel{!}{=} const. \tag{3}$$

If $\Delta\tilde{\nu}$ is sufficiently small, Eq. (3) simplifies to

$$E_{\tilde{\nu}}(T)\Delta\tilde{\nu} = const. \tag{4}$$

From Eq. (4) we construct a recursive formula for the sampling point distribution at temperature T

$$\tilde{\nu}_{i+1} = \tilde{\nu}_i + \frac{const}{E_{\tilde{\nu}_i}(T)}. \tag{5}$$

The first wavenumber $\tilde{\nu}_1$ and the constant *const* need to be specified. The procedure is started at $\tilde{\nu}_1 = 500\,{\rm cm}^{-1}$ (20μm). The overall number of sampling points N is controlled by the choice of *const*. A typical value is $const = 10^{-3}$, resulting in $N = 1000$ no matter which $T_{\rm OS}$ is considered. Fig. 1 shows the resulting (initial) wavenumber point distributions for selected temperatures $T_{\rm OS}$.

2.1. The final distribution

In order to be able to solve the radiative transfer throughout a stellar atmosphere we need a unique sampling point distribution which ideally holds for the whole temperature range of the stellar atmosphere. The temperatures under consideration are bracketed by 1000 K and 6000 K, the wavenumbers range from 500 cm^{-1} (20μm) to 5·10^4 cm^{-1} (0.2μm).

The unique sampling point distribution is constructed as follows: we first calculate separate, initial distributions for T=1000 K, 1500 K, 2000 K, . . . 6000 K and then take over those points from each distribution where $E_{\tilde{\nu}}(T)$ is maximum (open diamonds in Fig. 1).

Fig. 2 shows the number of wavenumber points in intervals of 400 cm^{-1} throughout the whole wavenumber range considered: the contribution from the normalized 1000 K Planck distribution function has a 10-times higher sampling point density than the contribution from the normalized 6000 K Planck

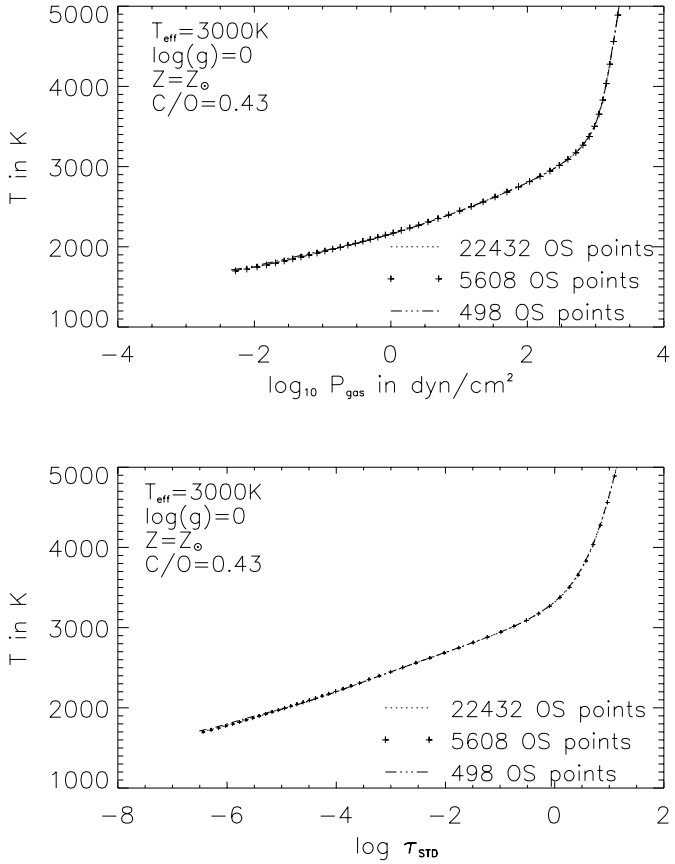

Fig. 3. The oxygen rich reference model with $Z = Z_{\odot}$ compared to model atmospheres computed with 5 608 and 498 sampling points.

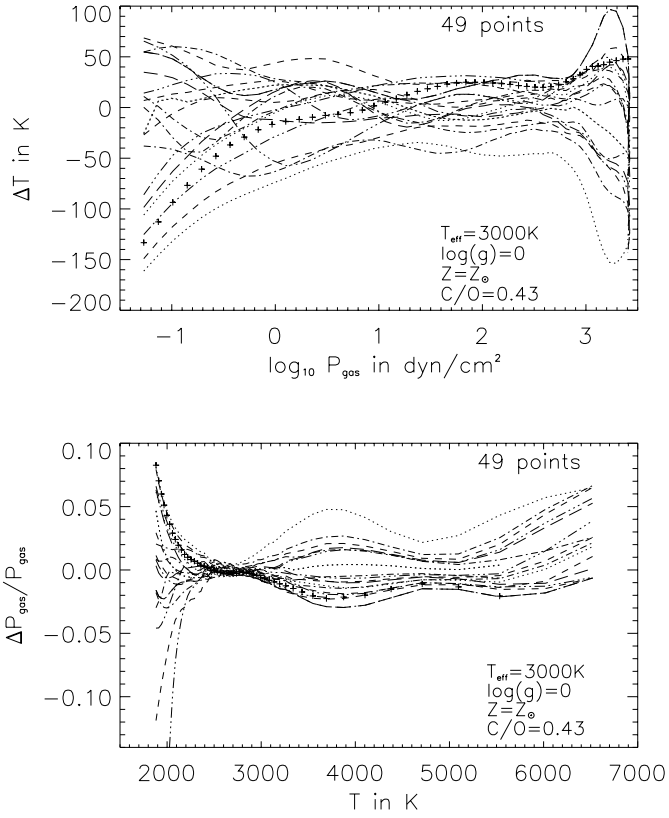

Fig. 4. Temperature and relative pressure differences, ΔT and $\Delta P_{\rm gas}/P_{\rm gas}$, for the oxygen rich 49 points model subset (see text) with $Z = Z_{\odot}$. The crossed line indicates the 49 random points model.

distribution. The distribution shown in Fig. 2 is the sampling point distribution we use in the opacity sampling program and for defining reference models. The distribution contains 22 432 points.

Furthermore, this proposed final wavenumber distribution automatically accounts for the fact that at lower temperatures a huge number of molecular lines dominate the opacity, whereas the opacity at high temperatures is more "smooth" (e.g. H^- continuum opacity). In addition, it is a statistic distribution because we do not use (nor can find) a correlation between the location of our sampling points and the location of the absorption lines.

3. Computation of model atmospheres

3.1. The opacity sampling

The primary input for molecular opacity computations is given by extensive line lists which contain gf-values, excitation energies, the wavenumbers, and if necessary the isotopic shifts and transition quantum numbers. The resulting absorption coefficients are stored separately for each molecule at every sampled wavenumber ($\tilde{\nu}_i$) and every temperature considered.

The H_2O (Jørgensen & Jensen 1993), CO (Querci et al. 1974), and TiO (Jørgensen 1994a) line lists are sampled within the opacity sampling grid of 22 432 wavenumbers which are distributed according to the concept of the "covering" curve illustrated in Fig.1 (1000 K . . .6000 K, 500 cm^{-1} . . . $5 \cdot 10^4$ cm^{-1}).

For technical reasons, it was not possible to adopt the same dense 22 432-points distribution for the carbon-rich models. Already sampled data were used for CH, C_2, C_3, HCN, and C_2H_2. Those are sampled to a wavenumber grid of 5 363 as described in detail by Jørgensen et al. (1992). Also here, the wavenumber range between the maxima of the 1000 K and the 6000 K Planck distribution is sampled with a higher density than the remaining parts of the total wavenumber range.

3.2. The model atmosphere code

We use the MARCS model atmosphere program (Gustafsson et al. 1975) in an improved and updated version for cool star atmospheres (Jørgensen et al. 1992). The MARCS code yields the hydrostatic T-$P_{\rm gas}$ structure of a stellar atmosphere for given effective temperature $T_{\rm eff}$, surface gravity g, and elemental abundances.[1] The atmospheric T-$P_{\rm gas}$ structure is obtained by assuming a static plane-parallel atmosphere in LTE and demanding radiative and convective equilibrium.

[1] The stellar mass is only needed if spherically symmetric model atmospheres are computed.

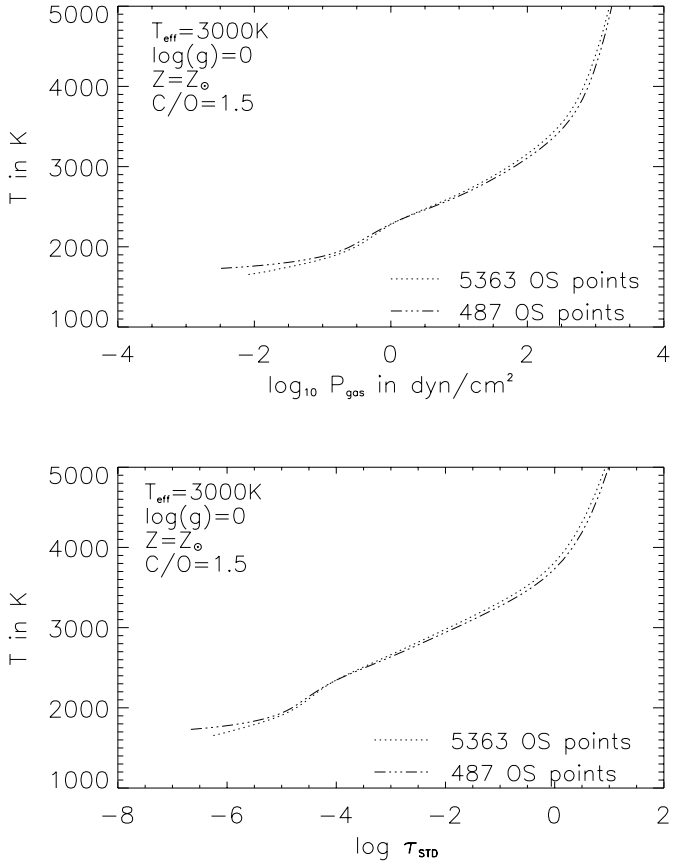

Fig. 5. The carbon rich reference model with $Z = Z_{\odot}$ compared to a model atmosphere computed with 487 sampling points.

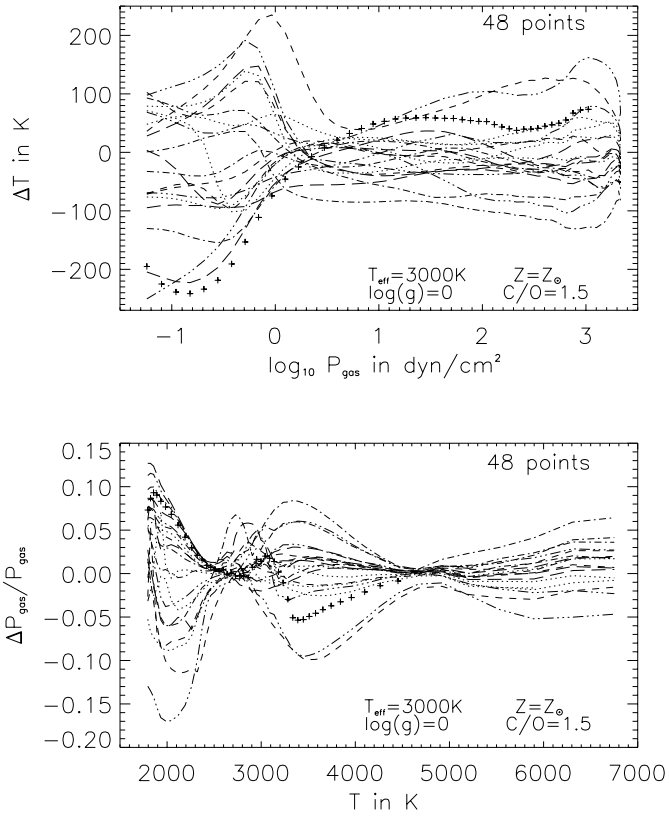

Fig. 6. Temperature and relative pressure differences, ΔT and $\Delta P_{\rm gas}/P_{\rm gas}$, for the carbon rich 48 points model subset (see text) with $Z = Z_{\odot}$. The crossed line indicates the random points model.

Elemental abundances are taken from Anders & Grevesse (1989), except for the Fe abundances taken from Holweger et al. (1990).

The models computed in this paper are divided into several subsets. Each subset is characterised by the number of wavenumber points and contains several model computations. In the oxygen-rich case, we computed models with 22 432 (the reference model), 5 608, 498, 101, 49, and 22 points. The wavenumber points of one subset are adopted from the original 22 432 points by selecting the fourth, the $45^{\rm th}$, the $222^{\rm nd}$, the $457^{\rm th}$, and the $1\,019^{\rm th}$ point. Models within one subset differ by starting at the first, second, third etc. point in the original 22 432 points set. Each subset is completed by including one model with a random choice of wavenumber points. All models (the latter to a lower degree of approximation) follow the sampling point distribution depicted in Fig.1.

The subsets for the carbon-rich case are constructed analogously. Carbon-rich model atmospheres are computed with 5 363 (the reference model), 487, 48, and 21 wavenumber points. Each subset is again completed by one model with a random choice of points.

All radiative quantities (i.e, $I_{\tilde{\nu}}, J_{\tilde{\nu}}, K_{\tilde{\nu}}, F_{\tilde{\nu}}$) are computed monochromatically without any averaging of the opacity.

For comparison, oxygen and carbon rich model atmospheres with the Rosseland mean opacity, straight mean opacities in 99 wavenumber intervals of $\Delta\tilde{\nu}$ =500 cm^{-1}, and a constant opacity value $\kappa_{\rm const} = 2 \cdot 10^{-4}$ cm^2/g (Bowen 1988) are computed. The Rosseland mean opacities are evaluated while executing the MARCS code. The straight mean opacities, $\kappa^i_{\rm str} = \int_{\tilde{\nu}_i}^{\tilde{\nu}_i + \Delta\tilde{\nu}} \kappa_{\tilde{\nu}} d\tilde{\nu} / \Delta\tilde{\nu}$ $(i = 1 \ldots 99)$, were computed for every molecule in advance and stored in a table.

In order to compare the different local temperatures and gas pressures between different model atmospheres, a standard optical depth scale $\tau_{\rm std} = \int_{\rm z}^{\rm z_{max}} \chi_{\rm std} dz$ ($\chi_{\rm std}$ continuum opacity at λ=8000Å) is defined. Such a standard optical depth is independent of the assumptions for the number and position of sampling points.

Theoretically, models computed with an infinite large number of sampling points provide the "correct" solution of the radiative transfer problem. For successively larger numbers of sampling points, the model structures (i.e. T-$P_{\rm gas}$, T-τ) are therefore expected to converge toward the correct model. Hence, our models with the largest number of sampling points are assumed to be "most correct".

4. Results

Hydrostatic model atmospheres were computed for

$T_{\rm eff}$=3000K, $\log(g)=0$, $Z=Z_{\odot}$, $C/O=0.43$ (Figs. 3, 4),
$T_{\rm eff}$=3000K, $\log(g)=0$, $Z=Z_{\odot}$, $C/O=1.5$ (Figs. 5, 6),

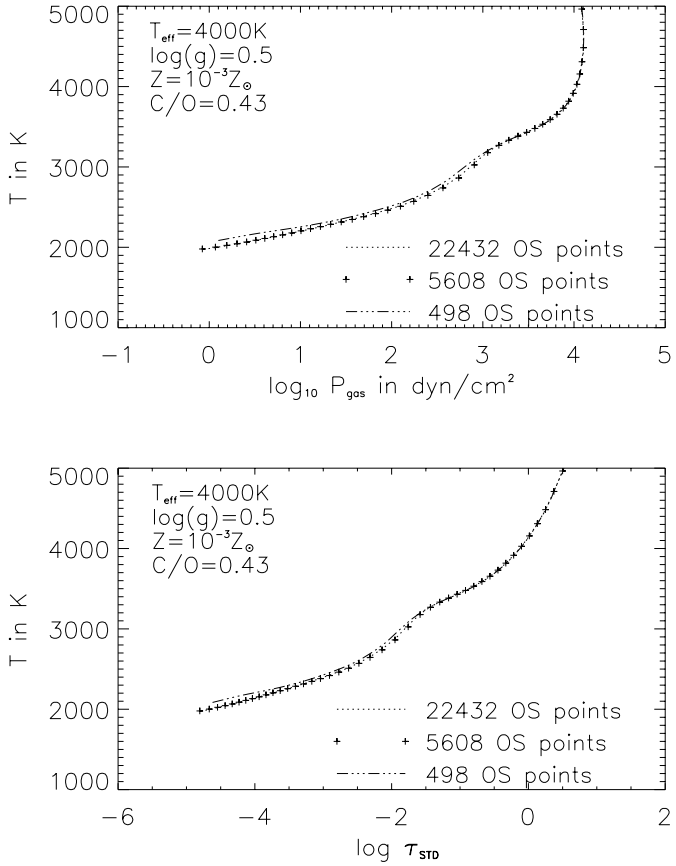

Fig. 7. The oxygen rich reference model with $Z = 10^{-3} Z_{\odot}$ compared to model atmospheres computed with 5 608 and 498 sampling points.

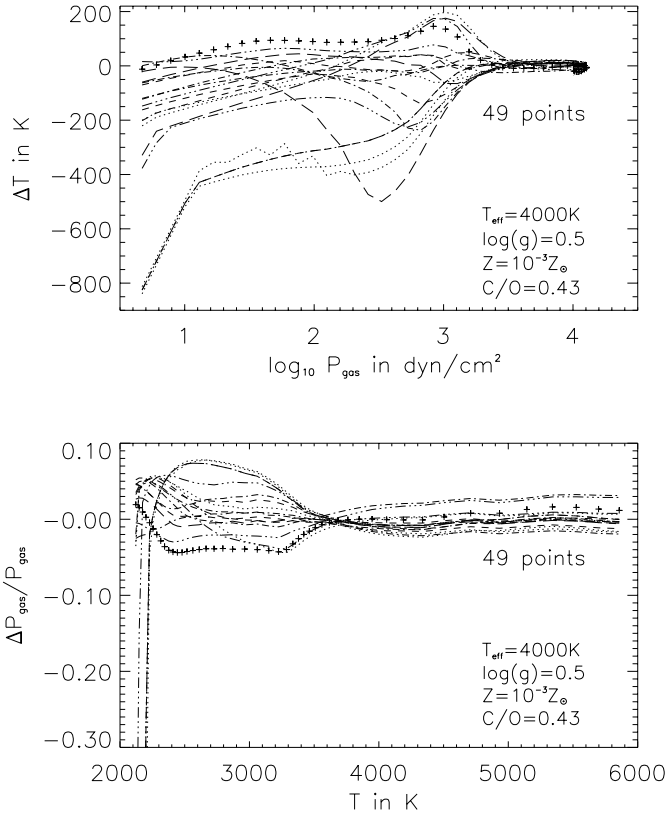

Fig. 8. Temperature and relative pressure differences, ΔT and $\Delta P_{\rm gas}/P_{\rm gas}$, for the oxygen rich 49 points model subset (see text) with $Z = 10^{-3} Z_{\odot}$. The crossed line indicates the random points model.

$T_{\rm eff}$=4000K, $\log(g)$=0.5,$Z=10^{-3} Z_{\odot}$,C/O=0.43 (Figs. 7, 8),
$T_{\rm eff}$=4000K, $\log(g)$=0.5,$Z=10^{-3} Z_{\odot}$,C/O=1.5 (Figs. 9, 10)

with different numbers of wavenumber points characterizing different subsets of model atmospheres.

Figs. 3 and 7 depict oxygen-rich model atmosphere structures computed with 22 432 (reference model), 5 608, and 498 points, Figs. 5 and 9 depict carbon-rich structures computed with 5 363 (reference model) and 487 sampling points. These figures show that deviations of less than 100 K occur between the reference models and those models with $N \approx 500$; largest in the carbon rich cases.

For convenience of the reader, we will only visualise the detailed structure of the deviations for the 50 points test models. The complete results are shown in Helling (1996; Appendix B). However, the maximum deviations in temperature and pressure for all model subsets considered are summarised in Table 1.

The upper panels of Figs. 4, 6, 8, and 10 depict the local temperature difference ΔT as function of the gas pressure $P_{\rm gas}$ of the reference model. ΔT is the difference between the local atmospheric temperature of the reference model and the local atmospheric temperature of the test model at the same standard optical depth $\tau_{\rm std}$, $T_{\rm ref}(\tau_{\rm std}) - T_j^N(\tau_{\rm std})$ with j=1 ... M (M is the number of models with N sampling points). $T_j^N(\tau_{\rm std})$ is the temperature of the $j^{\rm th}$ model from the subset with N sampling points at the standard optical depth $\tau_{\rm std}$. A negative temperature difference ΔT indicates that the test model is hotter than the reference model at respective optical depth $\tau_{\rm std}$.

The lower panels of Figs. 4, 6, 8, and 10 depict gas pressure differences $\Delta P_{\rm gas}$ relative to the reference model's gas pressure $P_{\rm gas}$ as function of the reference model's local temperature T. $\Delta P_{\rm gas}$ is the difference between the gas pressure of the reference model and the gas pressure of the test model at the same standard optical depth $\tau_{\rm std}$, $P_{\rm gas,ref}(\tau_{\rm std}) - P^N_{\rm gas,j}(\tau_{\rm std})$.

The temperature and pressure deviations increase remarkably in the surface layers of the photospheric models if fewer and fewer sampling points are used. Most of the $\approx$50 points models are much too hot in these regions of small optical depth. This effect increases for fewer sampling points because the important surface cooling due to strong absorption lines is not efficient any more. Metal poor models with such small numbers of sampling points approach the grey atmosphere in the outer and more diluted atmospheric layers.

Large deviations can be seen in the innermost regions of the photosphere of oxygen rich models with solar metallicity, and a minimum of almost no gas pressure deviation for all model subsets generally occurs at around 2800 K for $Z = Z_{\odot}$ and 3600 K for $Z = 10^{-3} Z_{\odot}$.

The random models (crossed lines in Figs. 4, 6, 8, 10) are among the most deviating models within each subset.

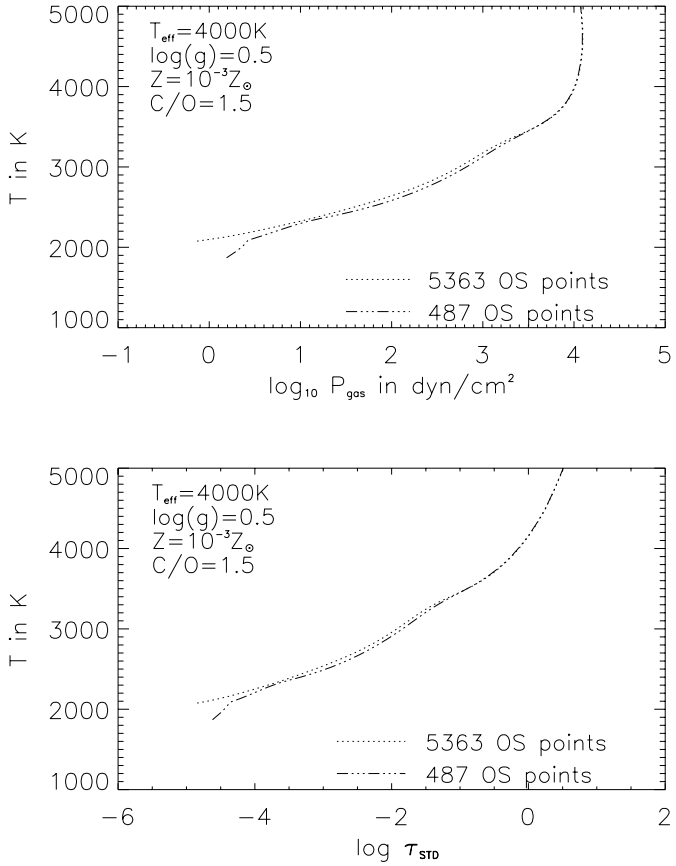

Fig. 9. The carbon rich reference model with $Z = 10^{-3} Z_{\odot}$ compared to a model atmosphere computed with 487 sampling points.

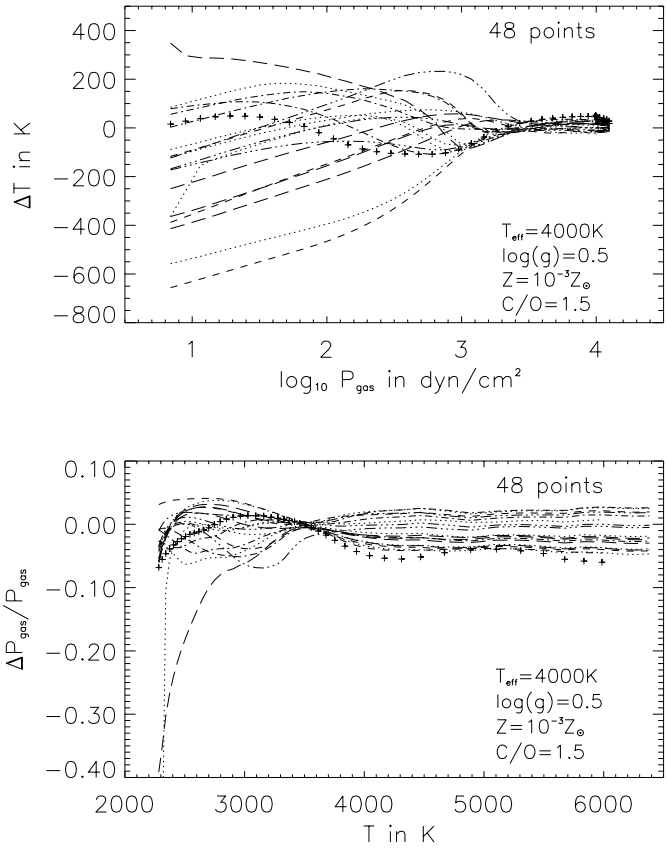

Fig. 10. Temperature and relative pressure differences, ΔT and $\Delta P_{\rm gas}/P_{\rm gas}$, for the carbon rich 48 points model subset (see text) with $Z = 10^{-3} Z_{\odot}$. The crossed line indicates the random points model.

The deviations will be further considered in terms of standard deviations

$$\sigma^N(\tau_{\rm std}) = \sqrt{\frac{\sum_{j=1}^{M} (T_{\rm ref}(\tau_{\rm std}) - T_j^N(\tau_{\rm std}))^2}{M}}, \qquad (6)$$

and 2-norms

$$\|T_{\rm ref} - T_j^N\|_2 = \sqrt{\frac{\int_{\log \tau_{\rm std}^{\rm min}}^{\log \tau_{\rm std}^{\rm max}} \mid T_{\rm ref}(\tau_{\rm std}) - T_j^N(\tau_{\rm std}) \mid^2 d \log \tau_{\rm std}}{\log(\tau_{\rm std}^{\rm max}/\tau_{\rm std}^{\rm min})}}. \qquad (7)$$

While the standard deviation is a statistical tool that allows to consider the mean, quadratic weighted, error at each $\tau_{\rm std}$ (see Figs. 13, 14), the 2-norm allows to consider the difference between the $j^{\rm th}$ model and the reference model in a whole interval of optical depth [$\tau_{\rm std}^{\rm min}$, $\tau_{\rm std}^{\rm max}$] and gives insight in the spread of deviation among the models belonging to one subset of N sampling points (see Figs. 11 and 12).

Figs. 11 and 12 show that the temperature deviations of individual models from the reference model become larger for smaller N, and demonstrates the spread of deviations to be expected for each of the model subsets. The spread for the metal-poor models is almost always larger than for the models with solar metallicity except for $N \approx 5\,608$ caused by the model with the random sampling point distribution.

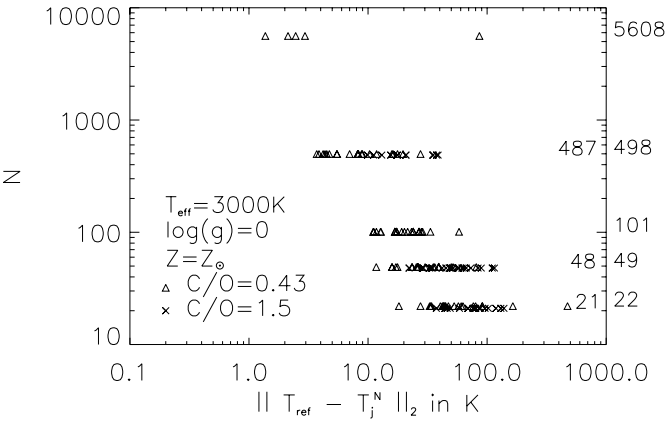

Fig. 11. 2-norms concerning temperature deviations for $Z = Z_{\odot}$ model subsets

Considering the standard deviation of the temperature $\sigma^N(\tau_{\rm std})$ as function of optical depth $\tau_{\rm std}$ (cf. Fig. 13, 14), the deviation increases with decreasing number of sampling points, and $\sigma^N(\tau_{\rm std})$ is especially large in the surface layers. The standard deviation indicates the mean maximum error at each $\tau_{\rm std}$ using N sampling points. For instance, the values of maximum

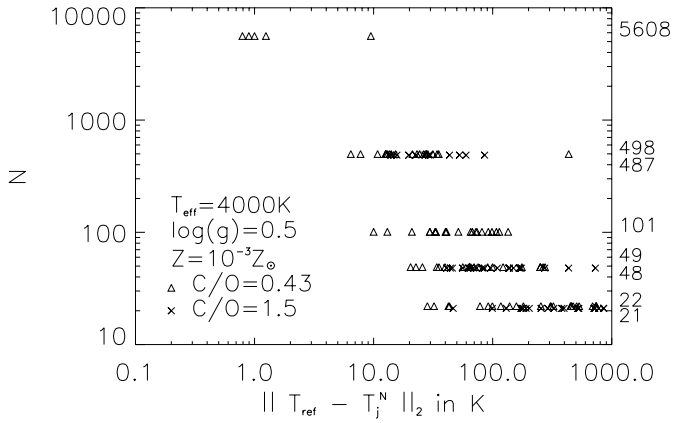

Fig. 12. 2-norm concerning temperature deviations for $Z = 10^{-3}Z_{\odot}$ model subsets

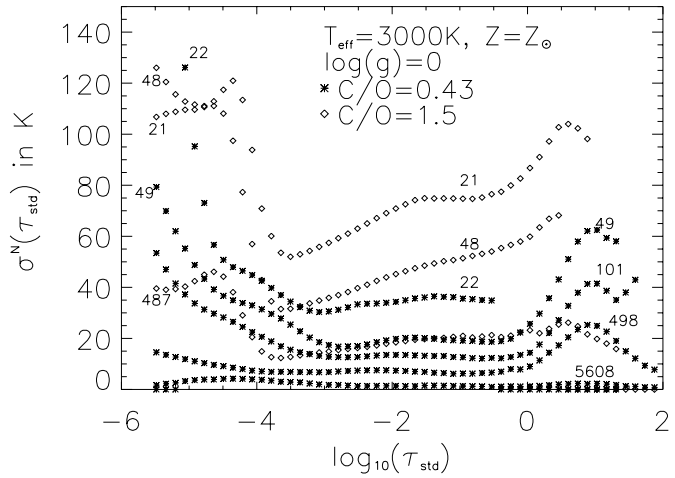

Fig. 13. Standard deviations: a comparison among models with $Z = Z_{\odot}$

standard deviations with respect to $\tau_{\rm std}$ for the model subset with $N \approx 50$, $\sigma^N_{\rm max} = \max_{\tau_{\rm std}}\{\sigma^N(\tau_{\rm std})\}$, are

$$Z = 10^{-3}Z_{\odot}, C/O = 0.43: \quad \sigma^{49}_{\rm max} = 550\,{\rm K}$$
$$Z = 10^{-3}Z_{\odot}, C/O = 1.5 \ : \quad \sigma^{48}_{\rm max} = 400\,{\rm K}$$
$$Z = Z_{\odot}, \quad C/O = 0.43: \quad \sigma^{49}_{\rm max} = 75\,{\rm K}$$
$$Z = Z_{\odot}, \quad C/O = 1.5 \ : \quad \sigma^{48}_{\rm max} = 130\,{\rm K}$$

4.1. Discussion

Few-points-models for both, solar metallicity and metal poor hydrostatic atmospheres, show the strongest temperature and pressure deviations from the reference model in the outermost, coolest layers. These strong deviations occur because the line opacity carrying species reach their maximum partial pressures in these regions as opposed to the deeper layers where continuum sources (often H^-) usually dominate the opacity (cf. Fig. 15). In addition to the partial pressure of the opacity carrying species, different numbers and distributions of sampling points affect the total opacity. If the total opacity happens to be larger than in the reference model, the temperature in the underlying layers increases because of the backwarming effect causing a steep temperature gradient. The temperature in the upper layer will be lower due to the line blanketing and may cause the formation of additional line opacity carrying species which can enhance the total opacity which in return causes additional back-

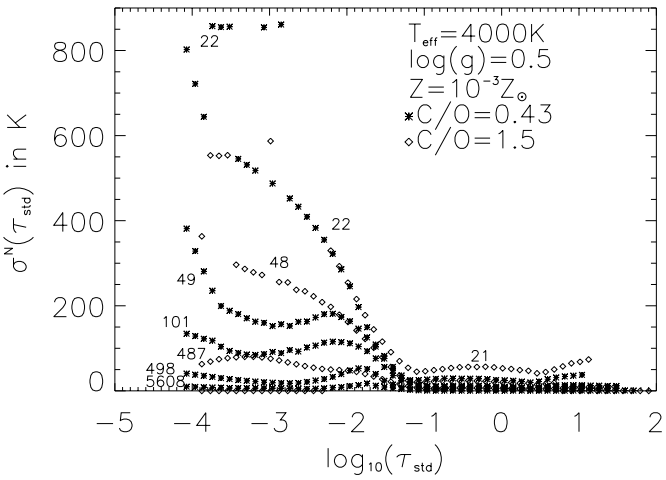

Fig. 14. Standard deviations: a comparison among models with $Z = 10^{-3}Z_{\odot}$

Table 1. OS model atmospheres: absolute maximum deviations for different numbers of wavenumber points N.
$\Delta T_{\rm surface}$ and $\Delta T_{\rm bottom}$ denote the maximum deviations found in the bottom and the surface layers of models with N sampling points. $\Delta T_{\rm global}$ and $\Delta P_{\rm gas,global}$ are the global maximum deviation in temperature and gas pressure, respectively.

Number of Points N	**5 608**	**498**	**101**	**49**	**22**
$T_{\rm eff}$=3000 K, $\log(g) = 0$, $Z = Z_{\odot}$, $C/O = 0.43$					
Number of Models M	5	22	23	21	22
$\Delta T_{\rm surface}$ in K	6	30	100	170	260
$\Delta T_{\rm bottom}$ in K	8	70	60	150	240
$\Delta T_{\rm global}$ in K	8	70	100	170	260
$\Delta P_{\rm gas,global}$ in %	0.3	2	6	12	$\gg$30
$T_{\rm eff}$=4000 K, $\log(g) = 0.5$, $Z = 10^{-3}Z_{\odot}$, $C/O = 0.43$					
Number of Models M	5	22	23	21	26
$\Delta T_{\rm surface}$ in K	2.5	80	250	840	1010
$\Delta T_{\rm bottom}$ in K	0.5	10	20	50	100
$\Delta T_{\rm global}$ in K	30	100	330	840	1010
$\Delta P_{\rm gas,global}$ in %	1.8	8	30	$\gg$30	$\gg$30
Number of Points N		**487**		**48**	**21**
$T_{\rm eff}$=3000 K, $\log(g) = 0$, $Z = Z_{\odot}$, $C/O = 1.5$					
Number of Models M		12		24	18
$\Delta T_{\rm surface}$ in K		100		250	300
$\Delta T_{\rm bottom}$ in K		50		160	180
$\Delta T_{\rm global}$ in K		100		250	300
$\Delta P_{\rm gas,global}$ in %		8.5		17	24
$T_{\rm eff}$=4000 K, $\log(g) = 0.5$, $Z = 10^{-3}Z_{\odot}$, $C/O = 1.5$					
Number of Models M		12		26	18
$\Delta T_{\rm surface}$ in K		220		660	900
$\Delta T_{\rm bottom}$ in K		20		50	50
$\Delta T_{\rm global,global}$ in K		220		660	900
$\Delta P_{\rm gas}$ in %		8		$\gg$30	35

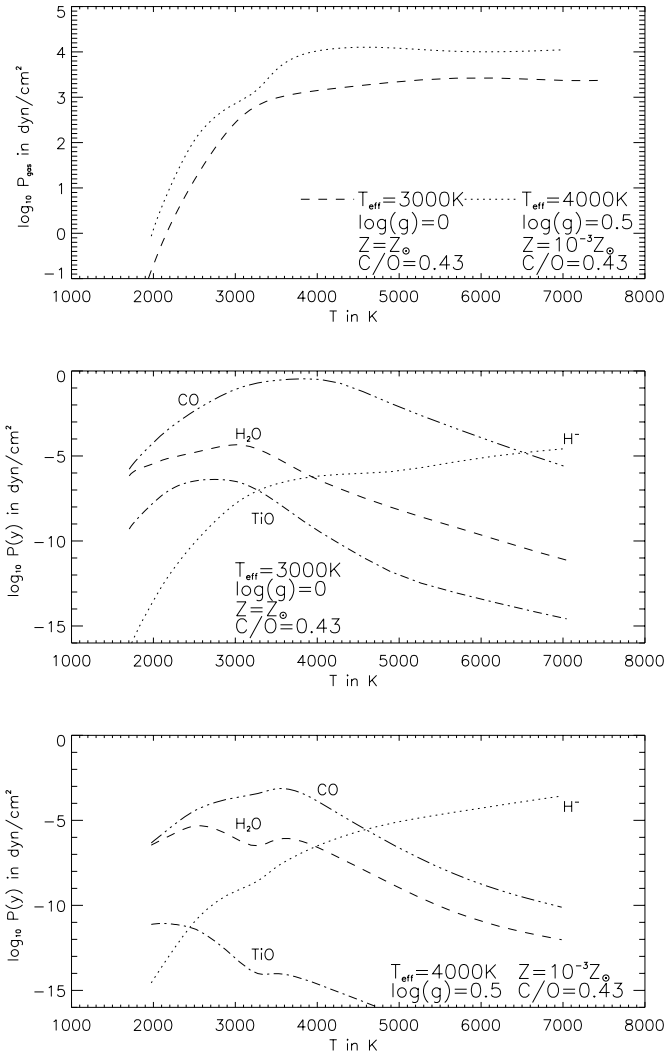

Fig. 15. The logarithmic partial pressures $\log_{10} P(y)$ of CO, H_2O, TiO, and H^- for oxygen rich stellar atmosphere with $Z = Z_\odot$ and $Z = 10^{-3} Z_\odot$. The most upper panel compares the corresponding T-$P_{\rm gas}$ structures.

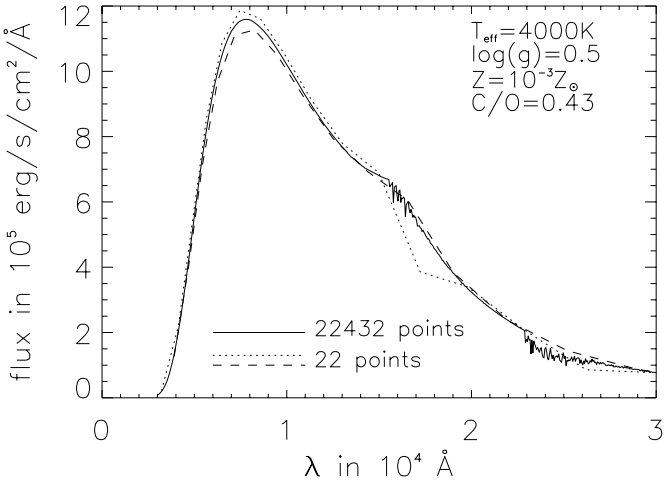

Fig. 16. The metal poor oxygen rich spectral energy distributions (SED). Compared is the 22 432 points reference model (smoothed in intervals of 50 Å) with two models computed with different distribution of 22 sampling points.

warming and line blanketing and so on. This self-amplifying effect could be the reason why the temperature deviations tend to increase outwards especially for smaller N.

Differences between solar metallicity and metal poor model atmospheres are partly caused by the stronger convection in metal poor atmospheres, but are mainly due to smaller line-blanketing. A typical example is CO. For solar metallicity, CO acts as an important surface cooler. The CO cooling rapidly diminishes for $\log Z < -2$ (Gustafsson et al. 1975). This change occurs when the CO concentration finally drops below a certain value where even its strongest lines do not contribute significantly.

The importance of TiO and H_2O decreases as well with decreasing metallicity, and although TiO has a larger absorption coefficient per molecule than H_2O has, its opacity decreases relatively to H_2O at low metallicities because it consists of two "metals". In the two lower panels of Fig. 15, the partial pressures $P(y)$ of the line opacity carrying species and the main continuum source H^- in oxygen rich atmospheres are depicted. In the metal-poor model (lowest panel), the partial pressure of H^- exceeds the partial pressures of CO, TiO and H_2O at $\approx$ 4500 K whereas in the solar metalictity model (middle panel), CO remains more abundant than H^- up to $\approx$ 7000 K. The same behavior is found in the carbon rich case for molecules important in such atmospheres not shown here.

Fig. 16 depicts the spectral energy distribution (SED) of the metal poor oxygen rich model with 22 432 points (solid line, smoothed in intervals of 50Å) and two models from the 22-point model subset (dotted and dashed lines). In fact, only the two CO overtone bands and very little from its groundstate are still visible at such low metalicities. The continuum opacities dominate the spectrum at all other wavelengths. The figure illustrates that, while one of the 22-point models (dotted) resembles the reference model's SED very well, the other (dashed) completely fails to account for the line absorption in the CO bands.

Most of the metal poor atmospheres computed with $N \leq 100$ result to be too hot because the probability to encounter the narrow CO bands becomes successively smaller if fewer sampling points are included (cf. Fig. 13, 14, 16). A hand-tuned enhancement of the spectral resolution of these bands might improve the accuracy of the metal poor, few-point models.

5. Comparison to mean opacity calculations

We compare model atmospheres computed with the full opacity sampling treatment to grey model atmospheres using the Rosseland mean $\kappa_{\rm R}$ and a constant opacity ($\kappa_{\rm const}$=$2 \cdot 10^{-4}$cm^2/g, Bowen 1988), and to models obtained by using straight mean opacities. The deviations are summarised in Table 2.

The model parameters are $T_{\rm eff}$=3000 K, $\log(g) = 0$, Z=$Z_\odot$ for $C/O = 0.43$ and $C/O = 1.5$.

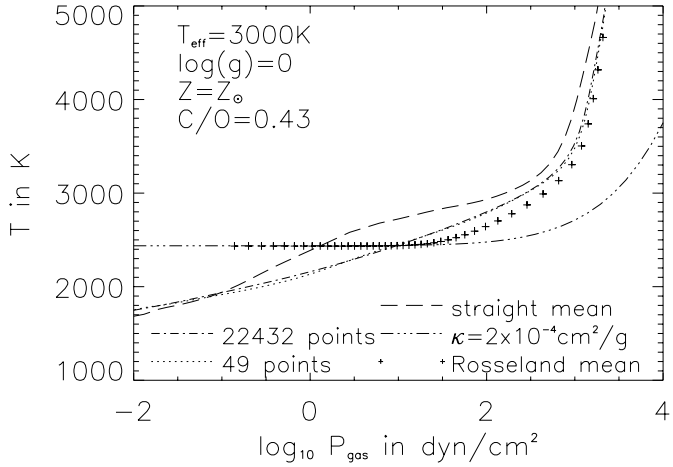

Fig. 17. Different opacity treatment in oxygen rich model atmospheres. The model with $N = 49$ (dotted) shows much smaller deviation (almost non) from the reference model with $N = 22\,432$ (dash-dot) than the mean-opacity models.

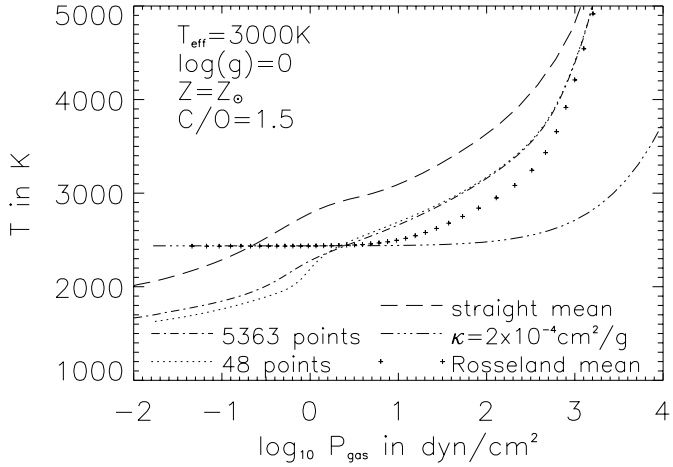

Fig. 18. Different opacity treatment in carbon rich model atmospheres. The model with $N = 48$ (dotted) shows much smaller deviation from the reference model with $N = 5\,363$ (dash-dot) than the mean-opacity models.

The Rosseland mean absorption coefficient $\kappa_{\rm R}$ is computed including CO, TiO and H_2O for oxygen rich models, and CO, CN, HCN, C_2, C_3 and C_2H_2 in the carbon rich case using the reference model's numbers and distribution of sampling points.

In general, the models obtained by a grey solution of the radiation transport problem predict a too hot outer atmosphere compared to opacity sampled models due to the line-blanketing effect. In the cases shown in Figs. 17 and 18, the grey temperature decreases outward to the well-known limit of $0.811\ T_{\rm eff}-$ no matter which type of grey opacity is used. This effect of missing line blanketing is especially illustrative when plane-parallel atmosphere models are considered because no geometrical effect leads to an outward decrease of temperature as in spherically symmetric atmosphere models. The only reason for the temperature decrease below $0.811\ T_{\rm eff}$ in plane-parallel models is line blanketing.

Table 2. Mean opacity model atmospheres: maximum temperature deviations

$T_{\rm eff}$=3000 K, $\log(g) = 0$, $Z = Z_\odot$				
	$C/O = 0.43$		$C/O = 1.5$	
	surface	bottom	surface	bottom
Rosseland mean	450 K	-250 K	650 K	-300 K
$\kappa_{\rm const} = 2 \cdot 10^{-4}$cm^2/g	450 K	-2 750 K	650 K	-3 000 K
straight means in $\Delta\tilde{\nu}$ =500cm^{-1}	< 100 K	750 K	400 K	750 K

Solar metallicity model atmospheres based on $\kappa_{\rm R}$ fit the OS model atmosphere very well at the bottom of the atmosphere. Models computed with a constant value for the absorption coefficient show the worst agreement in general. The reason for this lies within the too low absorption compared to a line blanketed or even a Rosseland mean model atmosphere. As the optically thick inner regions are governed by the diffusion approximation which relates large absorption coefficients to large temperature gradients, the inner regions will be always much too cool if $\kappa_{\rm const}$ is used. Furthermore, the inner regions have much too high gas pressures for this grey models.

The model atmospheres computed with the straight mean absorption coefficients are warmer than the OS model atmosphere over the whole gas pressure range considered. Since the averaging procedure of the straight mean opacity fills the absorption minima that are responsible for carrying the bulk of the flux in the spectral intervals $\Delta\tilde{\nu}$, the straight mean leads to a smaller temperature gradient, and the atmosphere is systematically too hot throughout. The effect is stronger in the carbon rich than in the oxygen rich case and is caused by the more efficient cooling by carbon rich molecules as compared to the oxygen rich gas, where in fact TiO rather heats than cools (Jørgensen 1994b).

In Fig. 17 and 18, we additionally show model atmospheres computed with $N \approx 50$ (dotted). These 50-point models are chosen from the subset such that their temperature deviations are representative (i.e. with deviations of the order of the standard deviation shown in Fig. 13). As can be seen from the figures, all the mean or constant opacity models deviate much more from the reference model than a model with $N \approx 50$.

6. Conclusions

Assuming that a statistical distribution of frequency (or wavenumber) points in the opacity sampling method resembles the mean intensity in a stellar atmosphere, we have calculated a composed Planckian sampling point distribution with characteristic temperatures between 1000 K and 6000 K and wavenumbers from 500 cm^{-1} (20μm) to 5·10^4 cm^{-1} (0.2μm).

The quality of an adopted opacity sampling is strongly dependent on the selection of the frequency points and by the completeness of the underlying absorption coefficients.

We computed several model atmospheres with fewer and fewer sampling points and examined the resulting changes in the atmospheric structures in order to define the limit of the opacity sampling method.

The 22 432 points frequency distribution we have argued for in this paper can be obtained by anonymous ftp to stella.nbi.dk (use your email address as password) with cd to pub/scan. All the distributions with fewer frequency points can be evaluated from the 22 432 points distribution as described in paragraph 3.2. Also the line data which we have used for the presented opacity sampling are, or will become, available at this ftp site.

The major results of our investigations are:

1. Model atmospheres computed with ≈ 500 sampling points have temperature errors usually less than 100 K.
2. Model atmospheres with ≈ 50 sampling points reproduce the atmospheric structure much better than model atmospheres computed with mean opacities.
3. Small numbers of randomly chosen frequencies produce much larger errors than frequencies chosen to physically represent the energy distribution.

The most important conclusion is:

– Hydrodynamic and stellar evolutionary models are usually computed by using simple mean opacity techniques. Considerable improvement of such simplified "mean-models" can be achieved by opacity sampling models with a very modest number of sampling points.

Acknowledgements. The authors thank the referee Dr. R.L. Kurucz for his comments on the manuscript. Ch. Helling warmly thanks Prof. E. Sedlmayr for making possible her stay at the Niels Bohr Institute in Copenhagen where most of this work has been done. Valuable comments from Dr. P. Woitke, Dr. A. Borysow, and Dr. J.M. Winters are gratefully acknowledged.

References

Anders E., Grevesse N. 1989. Geochimica et Cosmochimica 53, 197.
Bowen G. H. 1988. ApJ 329, 299.
Carbon D. F. 1984. in Methods in Radiative Transfer, Kalkofen W. (ed). Cambridge University Press.
Ekberg U., Eriksson K., Gustafsson B. 1986. A&A 167, 304.
Fleischer A. J., Gauger A., Sedlmayr E. 1992. A&A 266, 321.
Gustafsson B., Bell R. A., Eriksson K., Nordlund Å. 1975. A&A 42, 407.
Helling C. 1996. Diploma Thesis, Niels Bohr Institut Copenhagen, Technical University Berlin.
Höfner S., Dorfi E. A. 1997. A&A 319, 648.
Holweger H., Heise C., Kock M. 1990. A&A 232, 510.
Jørgensen U. G. 1994a. A&A 284, 179.
Jørgensen U. G. 1994b. in Molecules in the Stellar Environment, Lecture Notes in Physics, Jørgensen U. G. (ed). Springer Verlag Berlin.
Jørgensen U. G., Jensen P. 1993. Journal of Molecular Spectroscopy 161, 219.
Jørgensen U. G., Johnson H. R., Nordlund Å. 1992. A&A 261, 263.
Kurucz R. L. 1979. ApJS 40, 1.
Peytremann E. 1974. A&A 33, 203.
Plez, B. Brett J. M., Nordlund Å. 1992. A&A 256, 551.
Querci F. R., Querci M., Tsuji T. 1974. A&A 31, 265.
Salaris M., Chiffi A., Straniero O. 1993. ApJ 414, 580.
Sneden C., Johnson H. R., Krupp B. 1976. ApJ 204, 281.
VandenBerg D. A. 1983. ApJSS 51, 29.
Winters J. M., Fleischer A. J., Gauger A., Sedlmayr E. 1994. A&A 290, 623.
Winters J. M., Fleischer A. J., Le Bertre T., Sedlmayr E. 1997. A&A 326, 305.